Folding and Crumpling Adaptive Sheets

Rahul Narain Tobias Pfaff James F. O'Brien

University of California, Berkeley

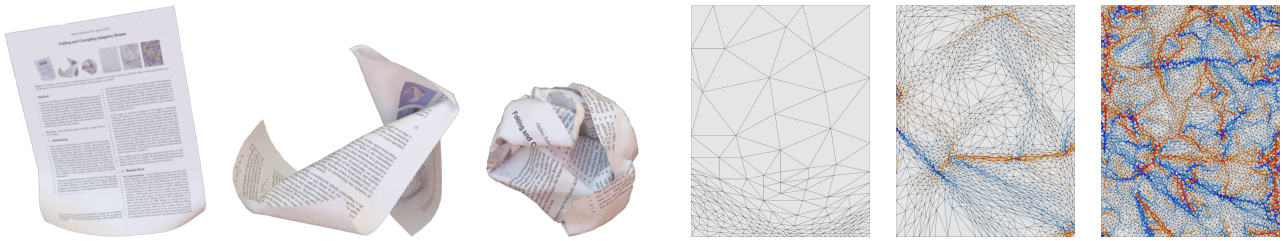

Figure 1: *Crumpling a sheet of paper is a challenging process to simulate as it produces geometry with both sharp creases and smooth areas. We efficiently resolve the emerging detail in the material through adaptive remeshing.*

Abstract

We present a technique for simulating plastic deformation in sheets of thin materials, such as crumpled paper, dented metal, and wrinkled cloth. Our simulation uses a framework of adaptive mesh refinement to dynamically align mesh edges with folds and creases. This framework allows efficient modeling of sharp features and avoids bend locking that would be otherwise caused by stiff in-plane behavior. By using an explicit plastic embedding space we prevent remeshing from causing shape diffusion. We include several examples demonstrating that the resulting method realistically simulates the behavior of thin sheets as they fold and crumple.

Keywords: Cloth simulation, paper, thin sheets, plastic deformation, bending

CR Categories: I.3.7 [Computer Graphics]: Three-Dimensional Graphics—Animation; I.6.8 [Simulation and Modeling]: Types of Simulation—Animation.

Links: DL PDF VIDEO WEB CODE

1 Introduction

When subjected to deforming forces, thin sheets of stiff materials such as paper or sheet metal tend to crumple, forming distinctive patterns characterized by networks of sharp folds and cone singularities. These patterns form due to the interaction between low bending resistance and high in-plane stiffness. The high in-plane stiffness prevents the materials from smoothly deforming into non-developable configurations with non-zero Gaussian curvature, but the low bending resistance makes the material prone to buckling. As buckling occurs, ridges form intersecting structures that concentrate curvature at cone singularities and narrow folds, as can be seen in Figure 1. In some materials, this process may be further enhanced if significant bending causes damage, locally reducing the material's resistance to further deformation.

Although mathematical models of deformation and bending in thin sheets and shells have been developed extensively (*e.g.* [Bridson et al. 2003; Grinspun et al. 2003; Kilian et al. 2008]), efficiently modeling the formation of sharp folds remains a difficult problem. Realistic representation of the appearance and behavior of these near-singular features requires a very high-resolution discretization, but only in a localized area. Away from these features, the material is typically smooth and attempting to use the high resolution globally would be infeasibly inefficient. Further, even if high resolution can be concentrated at sharp features, stiff in-plane behavior causes the linear-basis triangle elements often used in graphics applications to exhibit locking. This phenomenon manifests for thin sheets as artificial resistance to bending when the edges of the discretization are not aligned with the bending direction.

In this paper, we describe extensions to the adaptive remeshing scheme of Narain et al. [2012] that accommodate crumpling and folding behaviors in sheets formed of stiff materials. Our contributions include the following.

- We describe a formulation for bending plasticity that accounts for damage and that preserves shape during remeshing (Section 3).
- To avoid excessive mesh refinement, we modify buckling anticipation to account for rib-stiffening (Section 4.1), and we provide a way for combining individual terms of the sizing metric that avoids excessive refinement (Section 4.2).
- Finally, we describe a simple post-remeshing projection step that eliminates the jittering that would otherwise occur when the discretization of stiff materials is modified (Section 4.3).

With these improvements, dynamic anisotropic remeshing can be applied to stiff sheets, automatically concentrating detail where folds form and aligning mesh edges along the folds to avoid undesirable locking artifacts, such as those shown in Figure 2.

2 Related Work

Thin sheet dynamics In the graphics literature, there has been a large amount of work on the simulation of cloth and other thin sheets of flexible material, for example [Baraff and Witkin 1998; Bridson et al. 2002; Choi and Ko 2002; Bridson et al. 2003; Grinspun et al. 2003; Narain et al. 2012], but these techniques usually do not consider plastic effects such as persistent wrinkles. Materials with

From the conference proceedings of ACM SIGGRAPH 2013. Appearing in ACM Transaction on Graphics Vol. 32, No. 4.

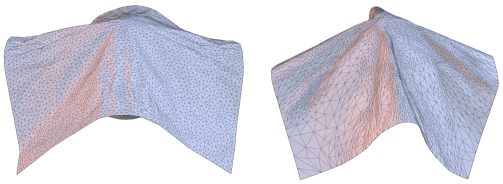

Figure 2: *A sheet with high in-plane stretching stiffness is dropped on a sphere. Locking creates artificial bending resistance when using a fixed isotropic mesh (left) but not when using adaptive anisotropic remeshing (right). Both simulations have an average of 8.77k faces.*

a high resistance to in-plane stretching require special treatment, because a stiff triangle mesh that is not aligned with the bending direction can cause locking. A fully inextensible material can be modeled through strain limiting [Provot 1995; Goldenthal et al. 2007; Thomaszewski et al. 2009; Wang et al. 2010] or the use of nonconforming elements [English and Bridson 2008], but dealing with materials that have high but finite in-plane stiffness is not addressed in these previous methods. In our work, we do not modify the finite element model, and instead avoid locking through the use of an adaptive mesh that conforms to the deformation of the material.

Plastic deformation and folding Animation of plastic deformation has previously focused mainly on volumetric objects [Terzopoulos and Fleischer 1988; O'Brien et al. 2002; Irving et al. 2004; Bargteil et al. 2007; Wojtan and Turk 2008; Wicke et al. 2010]. For thin shells, Gingold et al. [2004] presented an approch for simulating stretching and bending plasticity, as well as fracture, on non-adaptive meshes. We use a plasticity model similar to theirs, but also employ mesh adaptivity and a reference plastic embedding. As we show, these features are important components for modeling crumpled sheets with fine creases. Burgoon et al. [2006] simulated the creation of simple origami (paper folding) models; however, the fold edges had to be manually specified in advance, precluding the simulation of crumpling or wrinkles. Other approaches [Kilian et al. 2008; Rohmer et al. 2011; Solomon et al. 2012] allow geometric modeling and reconstruction of developable surfaces with curved folds, but do not address the dynamics of these surfaces.

Dynamic remeshing Previous work has established the importance of dynamically adapting the simulation mesh to capture fine details and faithfully represent plastic deformation. For elastic materials, Grinspun et al. [2002] advocated hierarchical refinement of finite element basis functions. Others have used dynamic remeshing of tetrahedral finite elements to simulate fluids [Klingner et al. 2006; Chentanez et al. 2007] and large viscoplastic flow [Bargteil et al. 2007; Wojtan and Turk 2008]. In this context, Wicke et al. [2010] introduced the use of a plastic embedding to minimize artificial diffusion of plastic deformation due to remeshing. Closely related to our work are remeshing techniques that have been used for cloth simulation [Hutchinson et al. 1996; Villard and Borouchaki 2002; Li and Volkov 2005; Simnett et al. 2009; Narain et al. 2012]. However, none of the existing methods deal with jittering, which is imperceptible for cloth but significant in stiffer materials; they also do not provide a way to accommodate plasticity in their remeshing process. In other related work, Brochu et al. [2012] demonstrated a robust collision handling technique for cloth simulation using adaptive meshes, and Busaryev et al. [2013] applied adaptive refinement for highly detailed simulation of tearing fracture in thin sheets.

Algorithm 1 Simulation loop with remeshing and plasticity.

```
for each frame do
    for each substep do
        implicit integration of internal and external forces
        perform plastic update using (2)-(3)
        update plastic embedding
        process collisions using impact zones
    perform remeshing and post-projection
    resample plasticity residuals
    output mesh
```

3 Elastoplastic Model for Thin Sheets

We represent a thin sheet of material as a finite element mesh composed of triangles. The initial flat rest shape of the sheet before deformation is stored in a two-dimensional parameter-space which defines the material coordinates $\mathbf{u}$ of each vertex. Each vertex also has a three-dimensional world space position $\mathbf{x}$ and world velocity $\mathbf{v}$. In-plane stretching forces are computed using Green strain, while bending forces use a discrete hinge model [Bridson et al. 2003; Grinspun et al. 2003] with nonzero rest angles θ_0 derived from plasticity information, as described below. Contact forces are handled using a combination of repulsion springs [Bridson et al. 2002] and impact zones [Harmon et al. 2008]. An overview of our simulation loop is shown in Algorithm 1. While implicit integration and collision resolution require small time steps on the order of 1 ms, we find that it is usually sufficient to perform remeshing only once per output frame (25 FPS in our examples).

We treat bending plasticity using a formulation based on the work of Gingold et al. [2004]. The plastic bending strain in the material is discretized as an initially zero 2×2 tensor $\mathbf{S}_p$ stored on faces. The *total* bending strain $\mathbf{S}$ of a face is determined from the hinge angles θ of its adjacent edges via

$$\mathbf{S} = \frac{1}{2A} \sum_{\text{adjacent edges } e} \theta_e \ell_e \mathbf{t}_e \mathbf{t}_e^{\mathsf{T}}, \tag{1}$$

where A is the area of the face, ℓ_e is the length of an edge and $\mathbf{t}_e$ is a unit vector perpendicular to the edge in parameter space. Yielding occurs whenever the elastic component of bending strain, $\mathbf{S}_e = \mathbf{S} - \mathbf{S}_p$, exceeds the material's yield curvature κ under the Frobenius norm. In that case, we update the plastic bending strain $\mathbf{S}_p$ via

$$\mathbf{S}_p \leftarrow \mathbf{S}_p + \frac{\mathbf{S}_e}{\|\mathbf{S}_e\|}(\|\mathbf{S}_e\| - \kappa). \tag{2}$$

The rest angles θ_0 used for computing bending forces at each edge are determined such that they would recover $\mathbf{S}_p$ when plugged into (1). This determination requires solving a small 3×3 linear system for each face. If adjacent faces disagree on the value of θ_0 for their common edge, we take the average.

To model materials such as paper that weaken when creased, we introduce a dimensionless scalar damage parameter δ which tracks the weakening of the material. When yielding occurs, we update δ on the face via

$$\delta \leftarrow \delta + \frac{1}{\kappa}(\|\mathbf{S}_e\| - \kappa). \tag{3}$$

The damage of an edge is taken to be the average of that of its adjacent faces. When computing bending forces, we attenuate the bending stiffness of the edge by $1/(1 + \gamma\delta)$, where γ is a parameter that describes the weakening behavior of the material. As demonstrated by the series of examples in Figure 3, a nonzero value of γ tends to give sharper creases due to strain concentrating further in

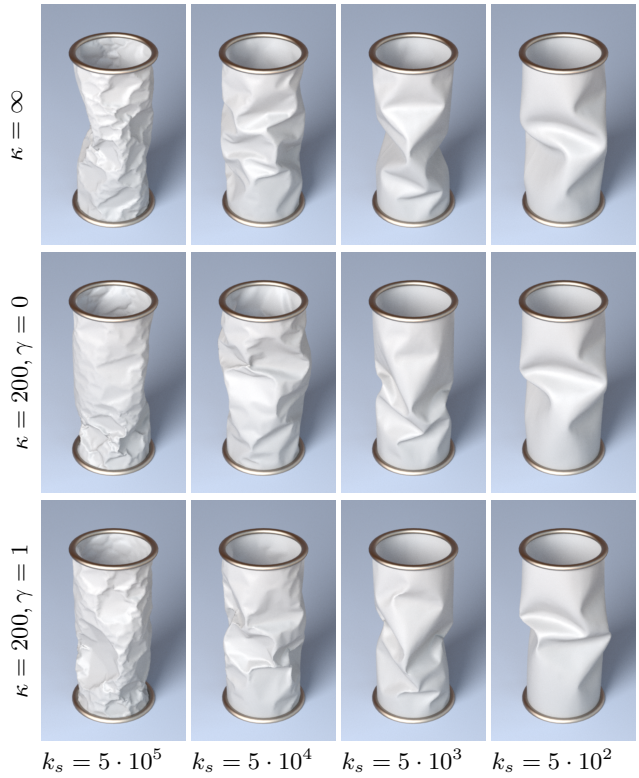

Figure 3: *These cylinders have constant bending stiffness* $k_b = 0.4 \times 10^{-3}\,\mathrm{N\,m}$ *and varying in-plane stretching stiffness in* $\mathrm{N\,m^{-1}}$*, and each is subjected to axial compression. From top to bottom, we show purely elastic behavior, plasticity without weakening, and plasticity with weakening.*

regions that have already yielded. The effect is significant for paper, as shown in Figure 1, where we used $\kappa = 200\,\mathrm{m^{-1}}$ and $\gamma = 1/2$.

After remeshing, we need to transfer the plastic strains of the new mesh. The naïve strategy of resampling via area-weighted averaging introduces undesirable diffusion, which would cause sharp creases and folds to blur out over time. To avoid this dissipation, we follow Wicke et al. [2010] in maintaining an additional plastic embedding of the mesh. As illustrated in Figure 4, this embedding stores as much of the plastic deformation as possible in a geometric representation.

We assign each vertex a three-dimensional position in the plastic space, such that the configuration of the material is as close as possible to its plastic rest state. In particular, we simply attempt to minimize the internal energy of the material, but with its in-plane stiffness down-weighted to allow non-developable plastic configurations. At each time step, after the plastic bending strain is modified via (2), we update the plastic embedding by performing one iteration of Newton's method with line search.

When the mesh topology is modified, we update the plastic embedding in a manner similar to the way Narain et al. [2012] update the world-space configuration: new vertices created by edge splits are assigned positions that optimize a smoothness term with respect to their neighboring faces. By preserving the shape of the plastic embedding, the remeshing procedure preserves plastic deformation as the mesh is resampled. However, there can remain a small amount of residual plastic strain that is not (or cannot be) represented in the plastic embedding, and must be resampled. Before remeshing, we determine the embedded bending strain $\tilde{\mathbf{S}}_p$ using the hinge angles in

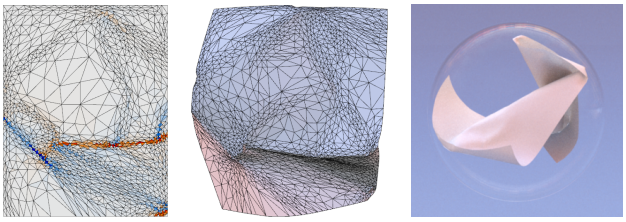

Figure 4: *From left to right: The parameter-space mesh, plastic embedding, and world-space configuration of a crumpled sheet of paper. In the parameter space mesh, faces are colored according to the trace of their plastic bending strain. Adaptive remeshing ensures that mesh edges align well with the direction of bending and creasing in the material.*

the plastic embedding space, and save the residual $\mathbf{S}_r = \mathbf{S}_p - \tilde{\mathbf{S}}_p$. After remeshing, we reconstruct $\mathbf{S}_p$ by resampling the residuals onto each new face through an area-weighted average over the old faces which overlap it. We set the damage δ for the new face directly by resampling.

4 Remeshing

Our remeshing scheme builds on the adaptive, anisotropic approach described by Narain et al. [2012] for cloth. We introduce modifications to the approach in order to accommodate stiff materials and plasticity. First, we introduce a post-remeshing projection step that prevents remeshing from causing rapid jittering artifacts. Without this step, remeshing is problematic for highly stiff materials, particularly where they are under compressive strain and newly introduced degrees of freedom can experience excessive instantaneous accelerations. Second, the plastic strain must be taken into account to preserve plastic deformation while remeshing. This accounting requires adding an additional term to the sizing criteria, and we describe a novel way to combine arbitrarily many such terms without causing excessive refinement. We also improve the buckling predictor to take into account rib-stiffening which can be a significant phenomenon in stiff materials.

For completeness, we briefly describe the basic remeshing algorithm as defined by Narain et al. [2012]. To control the desired shapes and sizes of mesh elements, one defines a "sizing field" $\mathbf{M}$ which is a symmetric 2×2 tensor field over the mesh vertices, based on criteria such as the local curvature, velocity gradient, and compressive strain. The sizing field determines the allowed lengths of mesh edges via the relation

$$\mathbf{u}_{ij}^{\mathsf{T}} \left(\frac{\mathbf{M}_i + \mathbf{M}_j}{2} \right) \mathbf{u}_{ij} \leq 1, \tag{4}$$

where $\mathbf{u}_{ij} = \mathbf{u}_i - \mathbf{u}_j$ is the parameter-space vector between two adjacent vertices. Edges which violate (4) are considered invalid and are split. Once all edges are valid, one collapses as many edges as possible without introducing new invalid edges. Throughout the remeshing process, edges are flipped to remain Delaunay relative to the anisotropy in $\mathbf{M}$.

The user controls the resolution of the adaptive mesh by specifying bounds on the per-face change in normals Δn, velocity difference Δv, and material compression c. The remeshing procedure computes a number of sizing terms on each face corresponding to these quantities, and combines them into a single sizing field $\mathbf{M}$ which guarantees that the new mesh's faces respect the specified bounds. After $\mathbf{M}$ is determined on faces, it is transferred to vertices by area-weighted averaging. This process smooths the $\mathbf{M}$ field, producing good mesh grading.

We differ from Narain et al. [2012] in the sizing terms we use and how we combine them. The terms for velocity variation,

$$\mathbf{M}_{\text{vel}} = (\nabla \mathbf{v})^T (\nabla \mathbf{v}), \tag{5}$$

and obstacle proximity,

$$\mathbf{M}_{\text{obs}} = \frac{1}{3} \sum_{i=1}^{3} \frac{(\mathbf{d}_i^T \nabla \mathbf{x})^T (\mathbf{d}_i^T \nabla \mathbf{x})}{\|\mathbf{d}_i\|^4}, \tag{6}$$

remain the same; here ∇ denotes the parameter-space gradient computed via the finite element basis, and $\mathbf{d}_i$ is the vector from the face's ith vertex to the nearest obstacle point. However, to preserve both elastic and plastic deformation, we include both the world-space (total) and plastic-space bending strain tensors $\mathbf{S}$ and $\mathbf{S}_p$ as sizing terms. If $\mathbf{S}_p$ were not taken into account, a creased material that was temporarily flattened in world space would become coarsened, degrading its stored plastic deformation. We also modify the buckling anticipation term, which we call $\mathbf{M}_{\text{buc}}$, so that it takes into account rib-stiffening effects as described in Section 4.1.

Given the user-specified bounds Δn, Δv, and c as above, we can guarantee that $\mathbf{M}$ respects the desired bounds if

$$\begin{gathered} \mathbf{M} \succeq \mathbf{S}/\Delta n^2, \quad \mathbf{M} \succeq \mathbf{S}_p/\Delta n^2, \\ \mathbf{M} \succeq \mathbf{M}_{\text{vel}}/\Delta v^2, \quad \mathbf{M} \succeq \mathbf{M}_{\text{buc}}/c^2, \\ \mathbf{M} \succeq \mathbf{M}_{\text{obs}}, \end{gathered} \tag{7}$$

where $\mathbf{A} \succeq \mathbf{B}$ denotes that $\mathbf{A} - \mathbf{B}$ is positive semidefinite, or equivalently, that $\mathbf{u}^\mathsf{T}\mathbf{A}\mathbf{u} \geq \mathbf{u}^\mathsf{T}\mathbf{B}\mathbf{u}$ for all $\mathbf{u} \in \mathbb{R}^2$. Previous work simply defined $\mathbf{M}$ as the sum of all terms, which can be inefficient: in the worst case, if all terms are equal, $\mathbf{M}$ will be five times as large as it needs to be. Instead, we find the optimal value of $\mathbf{M}$ using the procedure described in Section 4.2.

Edge flips are performed so that each edge is Delaunay in the stretched space induced by $\mathbf{M}$. An edge ij with adjacent vertices k and ℓ is Delaunay if

$$(\mathbf{u}_{jk} \times \mathbf{u}_{ik}) \mathbf{u}_{i\ell}^\mathsf{T} \mathbf{M}_{\text{avg}} \mathbf{u}_{j\ell} + \mathbf{u}_{jk}^\mathsf{T} \mathbf{M}_{\text{avg}} \mathbf{u}_{ik} (\mathbf{u}_{i\ell} \times \mathbf{u}_{j\ell}) \geq 0. \tag{8}$$

However, we do not always flip an edge whenever (8) is violated, because small changes in $\mathbf{M}$ can cause unnecessary flips when both an edge and its flipped version are close to Delaunay. Instead, we flip an edge only when the left-hand side of (8) falls below $-\alpha(\mathbf{u}_{jk} \times \mathbf{u}_{ik} + \mathbf{u}_{i\ell} \times \mathbf{u}_{j\ell})$ for a small value $\alpha = \frac{1}{10}$. This results in more temporally coherent meshes, improving the coherence of the simulation.

4.1 Rib-Stiffening

When a thin sheet experiences compressive stress, it is likely to buckle, trading in-plane elastic energy for bending energy. However, a curved sheet (such as one with corrugations) is significantly less likely to buckle perpendicular to the existing curvature, as doing so would require non-zero Gaussian curvature and a change in area. This rib-stiffening effect is an important feature of the dynamics of crumpling, as the compressive membrane strain in a crumpled sheet is concentrated at ridges of high curvature [Lobkovsky and Witten 1997].

To take this rib-stiffening effect into account, we make a heuristic argument described in Appendix A to estimate the scale at which a curved sheet will buckle. This argument suggests that the corresponding sizing term should be proportional to

$$\mathbf{M}_{\text{buc}} = \frac{1}{2} \left(-\varepsilon + \sqrt[\pm]{\varepsilon^2 - \frac{k_b}{4k_s} (\mathbf{R}\mathbf{S}\mathbf{R}^\mathsf{T})^2} \right)^+, \tag{9}$$

Algorithm 2 Finding the smallest disk enclosing a set of disks.

```
function MINIDISK(set of disks P, set of disks R [default ∅])
    if P = ∅ or |R| = 3 then
        return MD(R)
    choose disk D ∈ P
    disk E ← MINIDISK(P \ {D}, R)
    if E does not enclose D then
        E ← MINIDISK(P \ {D}, R ∪ {D})
    return E

function MD(set of disks R with |R| ≤ 3)
    if R = ∅ then
        return disk centered at origin with radius 0
    return smallest disk externally tangent to all disks in R
```

where ε is the membrane strain, and k_b and k_s are the bending and stretching stiffnesses of the material. Here $\sqrt[\pm]{\cdot}$ and $\cdot^+$ on a tensor denotes replacing each eigenvalue ξ with $\operatorname{sgn}(\xi)\sqrt{|\xi|}$ and $\max(\xi, 0)$ respectively, and $\mathbf{R}$ is a 90° rotation matrix. The resulting tensor $\mathbf{M}_{\text{buc}}$ equals the compressive strain $(-\varepsilon)^+$ used in previous work when $\mathbf{S} = 0$, and is smaller otherwise.

4.2 Combining Sizing Terms

With the addition of plastic strain, we have five different sizing terms to take into account during remeshing. Each term $\mathbf{M}_i$ corresponds to a constraint $\mathbf{u}^\mathsf{T}\mathbf{M}_i\mathbf{u} \leq 1$ on the allowed lengths of edges, and we wish to combine them into a single tensor $\mathbf{M}$ that guarantees that all constraints are satisfied.

One might consider an alternative approach of retaining all the $\mathbf{M}_i$ and performing edge splits when required by any of them (and collapses when allowed by all); however, that approach leaves open the choice of a single metric tensor for the edge flip criterion. Any choice will not be exactly compatible with the criteria used for splitting and collapsing, and in practice we find that it produces poor-quality meshes.

Therefore, we must find a single tensor $\mathbf{M}$ that best fits the intersection of all the constraints $\mathbf{u}^\mathsf{T}\mathbf{M}_i\mathbf{u} \leq 1$. This amounts to finding the smallest tensor $\mathbf{M}$ that dominates all of the $\mathbf{M}_i$, that is, such that $\mathbf{M} \succeq \mathbf{M}_i$ for all i. The tensors of interest, $\mathbf{M}_i$ and $\mathbf{M}$, are all symmetric 2×2 matrices. Any such matrix $\mathbf{A}$ can be written as

$$\mathbf{A} = a \begin{bmatrix} 1 & 0 \\ 0 & 1 \end{bmatrix} + b \begin{bmatrix} 1 & 0 \\ 0 & -1 \end{bmatrix} + c \begin{bmatrix} 0 & 1 \\ 1 & 0 \end{bmatrix}, \tag{10}$$

and is positive semidefinite if and only if $a \geq 0$ and $a^2 \geq b^2 + c^2$. We can associate these constraints with a disk $\mathcal{D}$ of radius a centered at (b, c); such a disk always contains the origin. Then $\mathbf{M}_1 \succeq \mathbf{M}_2$ if and only if $a_1 \geq a_2$ and $(a_1 - a_2)^2 \geq (b_1 - b_2)^2 + (c_1 - c_2)^2$, that is, disk $\mathcal{D}_1$ encloses disk $\mathcal{D}_2$.

Therefore, we choose $\mathbf{M}$ corresponding to the smallest disk that encloses all input disks $\mathcal{D}_i$. This is an LP-type problem that can be solved efficiently in linear time using a straightforward adaptation of Welzl's algorithm [Welzl 1991] described in Algorithm 2. It requires solving Apollonius' problem of finding a circle tangent to three given circles, which can be done through elementary means [Weisstein 2013].

4.3 Post-Remeshing Projection

Remeshing a stiff deformed sheet inevitably either produces changes in geometry that nudge the material away from dynamic equilibrium,

or introduces new degrees of freedom that are out of equilibrium. When the material's stiffness is high compared to its mass density these situations result in high instantaneous accelerations, causing jittering and unstable behavior as shown in the supplemental video.

Abstractly, we can view remeshing as a transformation from one finite-dimensional representation of the sheet to another. We would like this transformation to preserve the dynamical state of the sheet, in particular, the balance of forces acting on its parts. However, the remeshing procedure is oblivious to such considerations as it modifies the elements of the mesh. Therefore, after remeshing we must perform a projection step to bring the material to the configuration closest, in a dynamical sense, to its configuration before remeshing.

A simple way to describe the dynamical state of a material is through its instantaneous acceleration, which is directly proportional to the gradient of potential energy in configuration space. Using this criterion, we define the goal of our post-remeshing projection to be to adjust the world-space configuration of the mesh so that the instantaneous accelerations of its vertices match their corresponding values from before remeshing.

Let E denote the potential energy of the material due to internal and constraint forces. Immediately before the remeshing step, we compute the instantaneous acceleration

$$\mathbf{a}_i = -\frac{1}{m_i}\frac{\partial E}{\partial \mathbf{x}_i} \tag{11}$$

for each vertex and store it. During remeshing, this is averaged between the endpoints of split edges, and discarded for collapsed vertices. After remeshing, we seek the configuration where the same accelerations are attained, that is, every vertex satisfies

$$m_i \mathbf{a}_i = -\frac{\partial E}{\partial \mathbf{x}_i}. \tag{12}$$

This is equivalent to finding the stationary point of $E + \sum m_i \mathbf{a}_i \cdot \mathbf{x}_i$, or of finding the equilibrum under the influence of fictitious forces $-m_i \mathbf{a}_i$ at each vertex. However, this problem may be underconstrained (for example, if the sheet is in free space, any translation leaves the instantaneous accelerations unchanged) so we add a regularization term that prevents vertices from deviating far from their original positions. In full, the objective we minimize is

$$E + \sum m_i \mathbf{a}_i (\mathbf{x}_i - \mathbf{x}_i^0) + \sum \frac{\mu}{2} \|\mathbf{x}_i - \mathbf{x}_i^0\|^2, \tag{13}$$

where $\mathbf{x}_i^0$ is the unoptimized position of vertex i immediately after remeshing, and μ is the regularization parameter. The value of μ should be a small fraction of the stiffness of forces in the system; as we are modeling extremely stiff materials, we used $\mu = 10^3$.

Our method is similar to the approach taken by Spillmann and Teschner [2008] for adaptive refinement of one-dimensional elastic rods, but is more general as we do not assume that the material must be in static equilibrium. For solving the optimization, we use Newton's method. The first and second derivatives of E are simply the negation of the forces and Jacobians already used for implicit time integration, so very little additional implementation is required.

5 Results and Discussion

We have implemented these methods for modeling folding and crumpling sheets as an extension to the U.C. Berkeley ARCSim code for simulating adaptively refining and coarsening sheets. This code has been included as supplemental material and the most current version may be obtained from http://graphics.berkeley.edu/resources/ARCSim/.

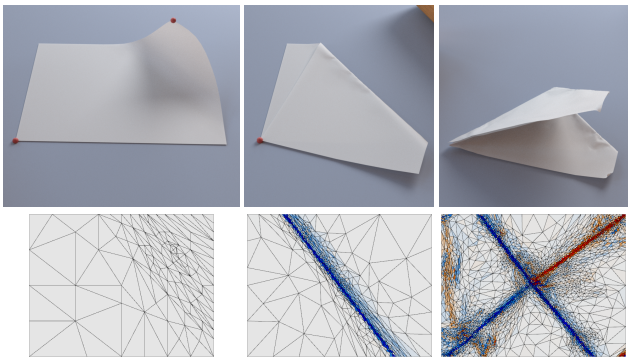

Figure 5: *Making two folds in a sheet of paper. After constraining the vertices, we roll a cylinder over the sheet to produce a sharp crease. Below each image, we visualize the corresponding simulation mesh in the flat parameterization space. Remeshing creates fine elements in detail regions and retains coarse elements in flat areas.*

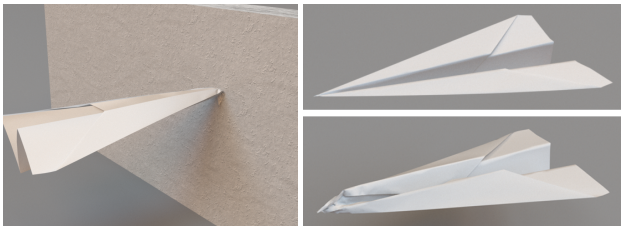

Figure 6: *A paper airplane crashes into a wall, denting its nose. On the right, we show the shape of the plane before and after the collision.*

Figure 1 shows a sheet of paper that has been crumpled inside a shrinking sphere. The substantial in-plane stiffness of the sheet causes it to resist deforming into a non-developable configuration, instead concentrating curvature into sharp folds that undergo permanent creasing. As shown in Figure 4, the simulation mesh automatically adapts to the deformation of the sheet, allowing these fine creases to be resolved when and where they appear. The creases are encoded implicitly in the shape of the mesh in the plastic space, allowing remeshing to take place without artificially diffusing the plastic deformation. If instead of rib-stiffening we use the compression term $\mathbf{M}_{\text{cmp}} = (-\varepsilon)^+$ from Narain et al. [2012], we get up to 2.08 times as many triangles. Similarly, simple addition of sizing terms gives 31.9% more triangles than our optimal combining scheme.

In Figure 3, we showed the classical example of a cylindrical sheet constrained at both ends being compressed axially. Depending on the ratio of bending to stretching stiffness, this may give rise to various characteristic buckling patterns. We show simulated results on this scenario for several stiffness ratios, exhibiting different behaviors similar to paper, metal and plastic.

To demonstrate the effectiveness of the algorithm in resolving fine creases and large flat regions simultaneously, we show in Figure 5 an example of a paper sheet being deliberately creased in two directions. After the first fold, the simulation mesh has extremely fine, narrow elements along the crease and large elements over the remaining smooth areas of the sheet. As one can observe by experimenting with a real sheet of paper, the presence of the crease makes perpendicular bending more difficult, and the second fold produces some secondary deformations in the sheet.

Figure 6 shows a paper airplane crashing into a wall. The sharp

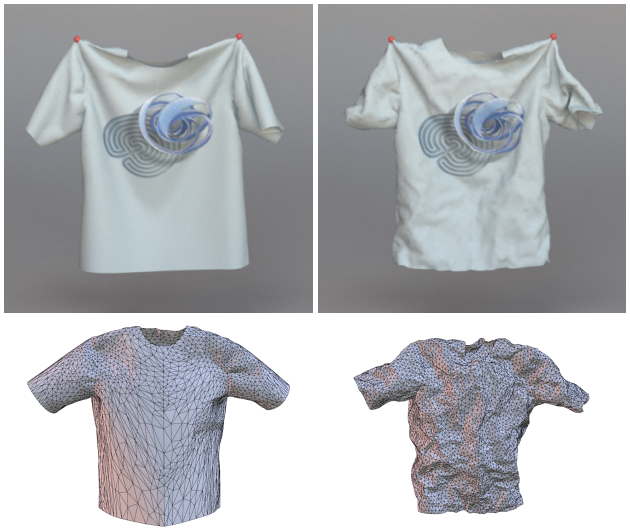

Figure 7: *A T-shirt before and after wrinkling. In the lower row, the visualizations of the plastic embedding shows the change in the rest pose of the shirt.*

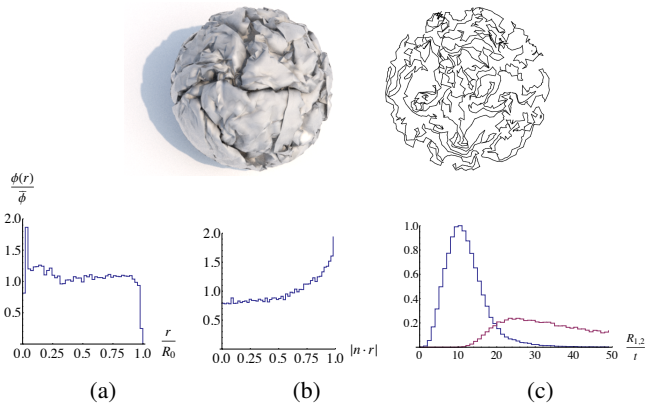

Figure 8: *Statistical properties of an aluminum sheet crumpled into a ball. Top row: A realistic rendering of the ball, and a cross section showing the internal structure. Bottom row: (a) Normalized volume fraction versus normalized distance from the center of mass. (b) The distribution of local orientation, quantified by the dot product $\hat{\mathbf{n}} \cdot \hat{\mathbf{r}}$ of the surface normal and the radial unit vector. (c) A normalized histogram of the first (blue) and second (red) principal curvature radii in units of thickness t.*

creases in the plane's folds are specified in the initial state, and are not diffused despite considerable changes in the mesh as the simulation proceeds. On the other hand, the nose of the plane deforms significantly and becomes dented.

Plastic deformation also serves as a good model for persistent wrinkles in cloth. In Figure 7, we have wrinkled an initially uncreased T-shirt by temporarily stuffing it tightly into a small box. The shirt develops a characteristic network of many fine wrinkles that remain after it is lifted out of its container.

Performance measurements for our examples are given in Table 1. Remeshing and projection form a small part of the total computational cost. We used the sparse Cholesky-based solver in the TAUCS library for solving the linear systems arising from implicit time integration and Newton's method. The constitutive model used for the T-shirt was the "Gray Interlock" material measured from real fabric by Wang et al. [2011].

5.1 Crumpling Comparison

We have performed a quantitative comparison of our simulation results with statistical properties of real crumpled sheets as measured by Cambou and Menon [2011] using high-resolution CT scans. Following their example, we simulated a disk-shaped aluminum sheet of radius $R_i = 5\,\text{cm}$, thickness $t = 25.4\,\mu\text{m}$ (slightly thicker than heavy-duty household foil), and yield curvature $\kappa = 1/(250t)$ that was crumpled into a ball of radius $R_o = 0.9\,\text{cm}$. The resulting compacted ball has an average volume fraction of $\phi = 6.5\%$ making it comparable to their $\phi = 6\%$ test. Due to limitations of our collision handling implementation we were not able to reproduce their densest experiment with $\phi = 22\%$. Doing so would require more robust collision handling, such as described by Ainsley et al. [2012], that could accommodate large stacks of arbitrarily close surfaces.

As shown in Figure 8, our results display substantial agreement with Cambou and Menon's observations. Compare the data plotted here in Figures 8(a), (b), and (c) with those plotted in red in Cambou and Menon's Figs. 2B, 3A, and 4B. The cross section shown by Cambou and Menon in Fig. 1A may be compared to the simulated cross section in Figure 8.

The mass of the simulated sheet is distributed nearly uniformly inside the ball with some irregularity near the center and a sharp falloff near the ball's boundary. Cambou and Menon report similar mass distribution, although they observe a slight upward trend away from the center before the falloff at ball's boundary.

The distribution of surface orientations is quantified by plotting the absolute value of the cosine between surface normal and the outward radial direction. For both our simulated ball and their physical ball the distribution of normals shows a bias towards surfaces normal to the radial direction. This bias is somewhat stronger for our simulated balls.

Curvature of the crumpled sheet is shown by plotting local values of the surface's two principal curvatures, R_1 and R_2. Consistent with Cambou and Menon, our data shows a distinct peak for $R_1 \approx 10t$, where t is the sheet's thickness. However, our plot of values for R_2 appears more similar to values they plot for $\phi = 22\%$ than for $\phi = 6\%$, and our peak is shifted further to the right.

Overall our data have good qualitative agreement with results reported by Cambou and Menon. Our animation of the crumpled foil sheet also matches well to our own informal observations taken while crumpling heavy-duty household foil. The differences between our data and those of Cambou and Menon are likely due to a combination of limitations in our simulation method, particularly collision handling, and possibly their measurement procedures.

5.2 Conclusions and Future Work

Crumpled paper provides an example of plastic deformation that is particularly challenging to simulate, as its high in-plane stiffness causes deformation to be concentrated along narrow creases and at point singularities. We have shown how dynamic remeshing can allow this behavior to be resolved accurately and efficiently by aligning mesh elements with the emerging detail in the material. Our contributions extend previous remeshing approaches to sheets of highly stiff materials, and allow plastic deformation to be accommodated faithfully in the remeshing process. The resulting technique

Name		Avg. #faces	Avg. time/frame (s) Integration	Plasticity	Collision	Remeshing	Projection	Total
Crumple[1]	(Fig. 1)	6.95k	61.6	14.9	75.0	0.42	13.9	168.8
Folds	(Fig. 5)	3.67k	9.43	7.28	4.31	0.14	1.67	22.8
Airplane	(Fig. 6)	2.07k	2.88	3.31	3.03	4.73	0.73	14.7
T-shirt[2]	(Fig. 7)	13.4k	21.7	6.55	16.0	0.49	–	44.7

Table 1: *Performance measurements for our examples. Notes:* [1]*The Crumple example runs slowly due to the large number of contacts.* [2]*We did not perform post-remeshing projection on the T-shirt, as perceptible jittering is not an issue with cloth's relatively low stiffness.*

realistically simulates a wide range of behaviors exhibited by thin sheets.

The computation time per frame can rise over time as more fine details appear in the material. It may be useful to automatically "freeze" certain minor creases if they would not have much dynamical effect, and thus allow the simulation mesh to be simplified. Whether this can be done without degrading the motion of the material is an interesting topic for future research.

Plastic bending of sheets is internally a very complex nonlinear phenomenon that is challenging to model accurately. We have used simplified plasticity and damage models which we feel serve the purposes of most graphical applications. We are interested in investigating more complex materials such as carbon-fiber epoxy composites, which exhibit very different behavior on yielding and for which accurate damage models are not yet well developed.

One potential problem with our damage model is that if a crease is formed and then forced to flatten out, the mesh may coarsen and cause the damage along the crease to diffuse over a larger area. This does not occur for the examples we tested, but it could happen with other materials. The problem could likely be avoided by adding a damage-based term to the sizing field.

Acknowledgments

The authors thank the following people who supported this work: Jonathan Shewchuk for invaluable discussions concerning remeshing and anisotropy; Huamin Wang for the use of his code and for insightful discussions; and Alexander Reshetov and Alexei Soupikov for helping with code optimization.

This work was supported by funding from the Intel Science and Technology Center for Visual Computing, NSF Grant IIS-0915462, UC Lab Fees Research Program Grant 09-LR-01-118889-OBRJ, and a gift from Pixar Animation Studios. Tobias Pfaff was supported by a Swiss National Science Foundation fellowship.

The images in this paper were rendered using the Mitsuba renderer by Wenzel Jakob.

References

AINSLEY, S., VOUGA, E., GRINSPUN, E., AND TAMSTORF, R. 2012. Speculative parallel asynchronous contact mechanics. *ACM Trans. Graph. 31*, 6 (Nov.), 151:1–151:8.

BARAFF, D., AND WITKIN, A. 1998. Large steps in cloth simulation. *Proc. SIGGRAPH '98*, 43–54.

BARGTEIL, A. W., WOJTAN, C., HODGINS, J. K., AND TURK, G. 2007. A finite element method for animating large viscoplastic flow. *ACM Trans. Graph. 26*, 3.

BRIDSON, R., FEDKIW, R., AND ANDERSON, J. 2002. Robust treatment of collisions, contact and friction for cloth animation. *ACM Trans. Graph. 21*, 3 (July), 594–603.

BRIDSON, R., MARINO, S., AND FEDKIW, R. 2003. Simulation of clothing with folds and wrinkles. In *Proc. 2003 ACM SIGGRAPH/Eurographics Symposium on Computer Animation*, SCA '03, 28–36.

BROCHU, T., EDWARDS, E., AND BRIDSON, R. 2012. Efficient geometrically exact continuous collision detection. *ACM Trans. Graph. 31*, 4 (July), 96:1–96:7.

BURGOON, R., GRINSPUN, E., AND WOOD, Z. 2006. Discrete shells origami. In *Proc. Computers And Their Applications*, 180–187.

BUSARYEV, O., DEY, T. K., AND WANG, H. 2013. Adaptive fracture simulation of multi-layered thin plates. *ACM Trans. Graph. (to appear)*.

CAMBOU, A. D., AND MENON, N. 2011. Three-dimensional structure of a sheet crumpled into a ball. *Proc. National Academy of Sciences of the United States of America 108*, 36 (Sept.), 14741–5.

CHENTANEZ, N., FELDMAN, B. E., LABELLE, F., O'BRIEN, J. F., AND SHEWCHUK, J. R. 2007. Liquid simulation on lattice-based tetrahedral meshes. In *Proc. ACM SIGGRAPH/Eurographics Symposium on Computer Animation 2007*, 219–228.

CHOI, K.-J., AND KO, H.-S. 2002. Stable but responsive cloth. *ACM Trans. Graph. 21*, 3 (July), 604–611.

ENGLISH, E., AND BRIDSON, R. 2008. Animating developable surfaces using nonconforming elements. *ACM Trans. Graph. 27*, 3 (Aug.), 66:1–66:5.

GINGOLD, Y., SECORD, A., HAN, J. Y., GRINSPUN, E., AND ZORIN, D. 2004. A discrete model for inelastic deformation of thin shells. Tech. rep., Courant Institute of Mathematical Sciences, New York University, Aug.

GOLDENTHAL, R., HARMON, D., FATTAL, R., BERCOVIER, M., AND GRINSPUN, E. 2007. Efficient simulation of inextensible cloth. *ACM Trans. Graph. 26*, 3 (July).

GRINSPUN, E., KRYSL, P., AND SCHRÖDER, P. 2002. CHARMS: a simple framework for adaptive simulation. *ACM Trans. Graph. 21*, 3 (July), 281–290.

GRINSPUN, E., HIRANI, A. N., DESBRUN, M., AND SCHRÖDER, P. 2003. Discrete shells. In *Proc. 2003 ACM SIGGRAPH/Eurographics Symposium on Computer Animation*, SCA '03, 62–67.

HARMON, D., VOUGA, E., TAMSTORF, R., AND GRINSPUN, E. 2008. Robust treatment of simultaneous collisions. *ACM Trans. Graph. 27*, 3 (Aug.), 23:1–23:4.

HUTCHINSON, D., PRESTON, M., AND HEWITT, T. 1996. Adaptive refinement for mass/spring simulations. In *7th Eurographics Workshop on Animation and Simulation*, Springer-Verlag, 31–45.

IRVING, G., TERAN, J., AND FEDKIW, R. 2004. Invertible finite elements for robust simulation of large deformation. In *Proc. 2004 ACM SIGGRAPH/Eurographics Symposium on Computer Animation*, SCA '04, 131–140.

KILIAN, M., FLÖRY, S., CHEN, Z., MITRA, N. J., SHEFFER, A., AND POTTMANN, H. 2008. Curved folding. *ACM Trans. Graph. 27*, 3 (Aug.), 75:1–75:9.

KLINGNER, B. M., FELDMAN, B. E., CHENTANEZ, N., AND O'BRIEN, J. F. 2006. Fluid animation with dynamic meshes. *ACM Trans. Graph. 25*, 3 (July), 820–825.

LI, L., AND VOLKOV, V. 2005. Cloth animation with adaptively refined meshes. In *Proc. 28th Australasian Computer Science Conference*, vol. 38.

LOBKOVSKY, A. E., AND WITTEN, T. A. 1997. Properties of ridges in elastic membranes. *Phys. Rev. E 55* (Feb), 1577–1589.

NARAIN, R., SAMII, A., AND O'BRIEN, J. F. 2012. Adaptive anisotropic remeshing for cloth simulation. *ACM Trans. Graph. 31*, 6 (Nov.), 152:1–152:10.

O'BRIEN, J. F., BARGTEIL, A. W., AND HODGINS, J. K. 2002. Graphical modeling and animation of ductile fracture. *ACM Trans. Graph. 21*, 3 (July), 291–294.

PROVOT, X. 1995. Deformation constraints in a mass-spring model to describe rigid cloth behavior. In *Proc. Graphics Interface 95*, 147–154.

ROHMER, D., CANI, M.-P., HAHMANN, S., AND THIBERT, B. 2011. Folded Paper Geometry from 2D Pattern and 3D Contour. In *Eurographics 2011 - Short Papers*, 21–24.

SIMNETT, T. J. R., LAYCOCK, S. D., AND DAY, A. M. 2009. An Edge-based Approach to Adaptively Refining a Mesh for Cloth Deformation. In *Eurographics UK Theory and Practice of Computer Graphics*, 77–84.

SOLOMON, J., VOUGA, E., WARDETZKY, M., AND GRINSPUN, E. 2012. Flexible developable surfaces. *Computer Graphics Forum 31*, 5 (Aug.), 1567–1576.

SPILLMANN, J., AND TESCHNER, M. 2008. An adaptive contact model for the robust simulation of knots. *Computer Graphics Forum 27*, 2, 497–506.

TERZOPOULOS, D., AND FLEISCHER, K. 1988. Modeling inelastic deformation: viscolelasticity, plasticity, fracture. In *Proc. SIGGRAPH '88*, 269–278.

THOMASZEWSKI, B., PABST, S., AND STRAER, W. 2009. Continuum-based strain limiting. *Computer Graphics Forum 28*, 2, 569–576.

VILLARD, J., AND BOROUCHAKI, H. 2002. Adaptive meshing for cloth animation. In *Proc. 11th International Meshing Roundtable*, Springer-Verlag, 243–252.

WANG, H., O'BRIEN, J. F., AND RAMAMOORTHI, R. 2010. Multi-resolution isotropic strain limiting. *ACM Trans. Graph. 29*, 6 (Dec.), 156:1–156:10.

WANG, H., O'BRIEN, J. F., AND RAMAMOORTHI, R. 2011. Data-driven elastic models for cloth: modeling and measurement. *ACM Trans. Graph. 30*, 4 (July), 71:1–71:12.

WEISSTEIN, E. W. 2013. Apollonius' problem. In *MathWorld—A Wolfram Web Resource*. Apr. http://mathworld.wolfram.com/ApolloniusProblem.html.

WELZL, E. 1991. Smallest enclosing disks (balls and ellipsoids). In *New Results and New Trends in Computer Science*, H. Maurer, Ed., vol. 555 of *Lecture Notes in Computer Science*. Springer Berlin Heidelberg, 359–370.

WICKE, M., RITCHIE, D., KLINGNER, B. M., BURKE, S., SHEWCHUK, J. R., AND O'BRIEN, J. F. 2010. Dynamic local remeshing for elastoplastic simulation. *ACM Trans. Graph. 29* (July), 49:1–49:11.

WOJTAN, C., AND TURK, G. 2008. Fast viscoelastic behavior with thin features. *ACM Trans. Graph. 27*, 3 (Aug.), 47:1–47:8.

A Buckling in Curved Sheets

Consider a square patch of material of size $\ell \times \ell$ with stretching and bending stiffnesses k_s and k_b, whose ends are constrained to have specified curvature s_{xx} and compressive strain ε_{yy}. Its internal energy per unit area in this configuration is

$$e_1 = k_s \varepsilon_{yy}^2 + k_b s_{xx}^2. \tag{14}$$

If it buckles into an arc to eliminate ε_{yy}, it will have an additional curvature $s_{yy} \propto \sqrt{\varepsilon_{yy}}/\ell$, but this will also produce an in-plane shear strain on the order of $\varepsilon_{xy} = s_{xx} s_{yy} \ell^2/4 = s_{xx}\sqrt{\varepsilon_{yy}}\ell/4$, giving a total internal energy per unit area of

$$\begin{aligned} e_2 &= k_s \varepsilon_{xy}^2 + k_b s_{xx}^2 + k_b s_{yy}^2 && (15)\\ &= \frac{1}{16} k_s \varepsilon_{yy} s_{xx}^2 \ell^2 + k_b s_{xx}^2 + k_b \varepsilon_{yy}/\ell^2. && (16) \end{aligned}$$

We anticipate the size of possible wrinkles by considering the range of ℓ for which buckling is energetically favorable, *i.e.* $e_2 \le e_1$. Letting $m = 1/\ell^2$, the smallest ℓ for which this holds corresponds to

$$m = \frac{k_s}{2k_b}\left(\varepsilon_{yy} + \sqrt{\varepsilon_{yy}^2 - \frac{k_b}{4k_s} s_{xx}^2}\right). \tag{17}$$

When the quantity D under the square root sign is negative, buckling is not favored at any scale. In this case, we find it useful to replace $\sqrt{D}$ with $-\sqrt{-D}$ to suppress refinement.

We extend this formula to tensor-valued quantities by applying it to the corresponding eigenvalues. As s_{xx} opposes ε_{yy} and vice versa, we take the "perpendicular" of the $\mathbf{S}$ tensor, namely $\mathbf{RSR}^\mathsf{T}$ where $\mathbf{R}$ represents rotation by $\pi/2$. The compression threshold $c_{\max}$ used by Narain et al. [2012] corresponds to the quantity $\sqrt{k_b/k_s}$ in our formula.